This is an open access article published under an ACS AuthorChoice License, which permits copying and redistribution of the article or any adaptations for non-commercial purposes.

ACS OMEGA

Article

Cite This: ACS Omega 2019, 4, 21559−21566

http://pubs.acs.org/journal/acsodf

Sodium, Potassium, and Lithium Complexes of Phenanthroline and Diclofenac: First Report on Anticancer Studies

Syed Raza Shah,[†,‡] Zarbad Shah,[‡] Ajmal Khan,[†] Ayaz Ahmed,[§] Sohani,[‡] Javid Hussain,[∥] Rene Csuk,[⊥] Muhammad U. Anwar,*[,†] and Ahmed Al-Harrasi*[,†]

[†]Natural and Medical Sciences Research Centre, [∥]Department of Biological Sciences and Chemistry, University of Nizwa, Birkat Almouz 616, Oman

[‡]Department of Chemistry, Bacha Khan University Charsadda, Charsadda-24420, Khyber Pakhtunkhwa, Pakistan

[§]Dr. Panjwani Center for Molecular Medicine and Drug Research, International Center for Chemical and Biological Sciences, University of Karachi, Karachi 75270, Pakistan

[⊥]Organic Chemistry, Martin-Luther-University Halle-Wittenberg, Kurt-Mothes-Str. 2, d-06120, Halle (Saale), Germany

Supporting Information

ABSTRACT: Diclofenac or 2-[(2′,6′-dichlorophenyl)-amino]phenyl}acetic acid (**dcf**) is a nonsteroidal anti-inflammatory drug, and 1,10-phenanthroline (**phen**) is a well-known enzyme inhibitor. In this study, three new alkali metal complexes (**1**−**3**) containing both **phen** and **dcf** were prepared, and their structures were characterized by a variety of analytical techniques including infrared and UV−vis spectroscopy, ^{1}H NMR and ^{13}C NMR elemental analysis, mass spectrometry, and single-crystal X-ray diffraction analysis. In these complexes, **phen** binds via a *N*,*N*′-chelate pocket, while the monoanionic **dcf**—ligand remains either uncoordinated (in the case of **1** and **3**) or coordinated in a bidentate fashion (in the case of **2**). All three complexes crystallize in the triclinic space group P-1. $[Na_2(\mathbf{phen})_2(H_2O)_4][\mathbf{dcf}]_2$ (**1**) is a dinuclear sodium complex, where two crystallographically identical Na^+ cations adopt a distorted five-coordinate spherical square-pyramidal geometry, with a $[N_2O_3]$ donor set. $[K_2(\mathbf{phen})_2(\mathbf{dcf})_2(H_2O)_4]$ (**2**) is also a dinuclear complex where the crystallographically unique K^+ cation adopts a distorted seven-coordinate geometry comprising a $[N_2O_5]$ donor set. $[Li(\mathbf{phen})(H_2O)_2][\mathbf{dcf}]$ (**3**) is a mononuclear lithium complex where the Li^+ cation adopts a four-coordinate distorted tetrahedral geometry comprising a $[N_2O_2]$ donor set. The complexes were evaluated for their anticancer activity against lung and oral cancer cell lines as well as for their antibacterial potential. The prepared complexes displayed very good antibacterial and anticancer activities with an excellent bioavailability.

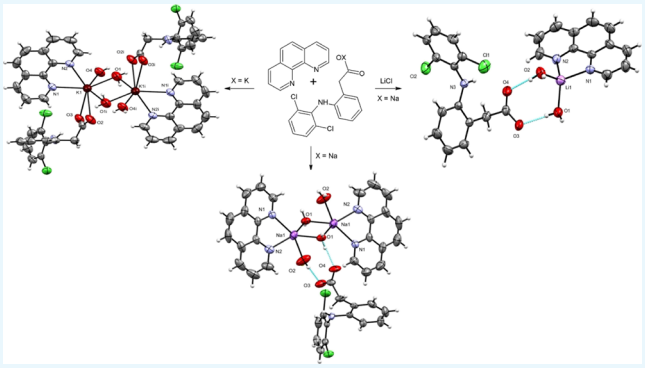

INTRODUCTION

Cancer morbidity and mortality is a worldwide phenomenon claiming 70% of the deaths out of 9.6 million deaths worldwide among low- and middle-income countries.[1] More than 60% of new emerging cancer cases are centered in Asian countries. Besides cancer, emerging antimicrobial-resistant pathogens are considered to be a major threat. The emergence of antimicrobial-resistant pathogens is likely to develop into a major health concern by 2050.[2] The efficacy of existing drugs is reducing globally day by day against bacterial pathogens because of the rise of antimicrobial resistance.[3] Different factors play a crucial role for the development of resistance such as multispecies biofilm modes of growth, genetic swapping, and mutation.[4] The increasing resistance of certain cancer lineages and microbial pathogens to existing treatments is proving a major challenge.[5] This situation requires exploring new stable chemical entities with better antimicrobial potential and less toxicity. In this respect, the coordination complexes received considerable attention because of their potential applications in the field of medicinal chemistry.[6]

Metal complexes interact with intracellular biomolecules and exhibit enzyme inhibition.[7] They increase lipophilicity, affect alteration of cell membrane functions, and arrest cell cycle.[8] In cancer chemotherapy, cisplatin and other platinum coordination compounds are among the most successfully used anticancer drugs.[9] Among coordination complexes, Schiff base complexes with first row transition and inner transition metals have been extensively studied for their potential in cancer therapy.[10] Much effort focused on transition metals, while anticancer studies on the complexes containing alkali

Received: October 8, 2019
Accepted: November 15, 2019
Published: December 3, 2019

© 2019 American Chemical Society

DOI: 10.1021/acsomega.9b03314
ACS Omega 2019, 4, 21559−21566

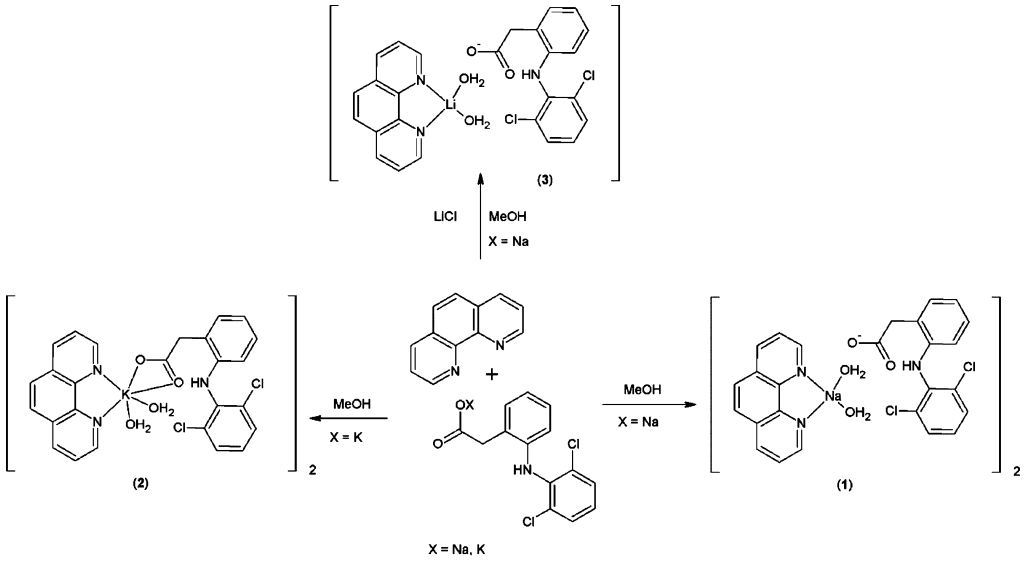

Figure 1. Synthetic routes to $[Na_2(\mathbf{phen})_2(H_2O)_4][\mathbf{dcf}]_2$ (**1**), $[K_2(\mathbf{phen})_2(\mathbf{dcf})_2(H_2O)_4]$ (**2**), and $[Li(\mathbf{phen})(H_2O)_2][\mathbf{dcf}]$ (**3**).

metals are still unknown. These metal ions play a vital role in various biological pathways such as cellular diversity, partition, apoptosis, homeostasis, adjusting electrolyte balances, pH, and nerve impulses.[11] The role of potassium and sodium concentration in cancer growth risk is the most important subject in cancer research.[12,13] Significant levels of sodium concentration have been found in cancer cells as compared to normal cells of the identical tissue,[14] while potassium on the other hand can offer a better solution for cancer immunotherapy.[13] Lithium ions are more efficient in facilitating many vital processes and cellular pathways by efficient penetration through cellular membranes.[15] Lithium has been used extensively for the therapeutic treatment of mood disorders.[15,16] Lithium can modify the biochemical functions of transcription factors, leading to important physiological or pathophysiological functions in cancer research.[17]

In the current study, three new alkali metal complexes with 1,10-phenanthroline (**phen**) and {2-[(2′,6′-dichlorophenyl)-amino]phenyl}acetate (**dcf**) are reported (Figure 1). **phen** is a well-known N-donor ligand with predictable coordination chemistry, offering a *N*,*N*′-chelate pocket for metal ions and is often employed with a range of O-donor coligands to produce a range of complexes with different structural topologies.[18−20] **phen** is also a well-known enzyme inhibitor.[21−23] The potassium and sodium salts of **dcf** (commonly known as diclofenac) are well-known nonsteroid anti-inflammatory drugs.[24] The coordination chemistry of **dcf** and **phen** with transition metals is known;[25,26] however, to date, no reports are published on alkali metal complexes with **phen**/**dcf** mixed ligand systems. As a continuation of our search for new potential bioactive compounds,[27] we have sought to combine the established enzyme inhibition properties of **phen** with the anti-inflammatory properties of **dcf** through the development of structurally well-defined alkali metal complexes of **phen**/**dcf** as potentially bioactive compounds. Specifically, we were interested in the anticancer and antibacterial activities of selected alkali metal complexes. We have investigated the reactions of **phen** with $\mathbf{dcf}^{-}\mathbf{M}^{+}$ (M = Na, K) and described the structures of the dinuclear complexes of both $[Na_2(\mathbf{phen})_2(H_2O)_4][\mathbf{dcf}]_2$ (**1**) and $[K_2(\mathbf{phen})_2(\mathbf{dcf})_2(H_2O)_4]$ (**2**) (Figure 1), while in the presence of LiCl, a mononuclear complex $\{[Li(\mathbf{phen})(H_2O)_2](\mathbf{dcf})\}$ (**3**) was isolated. The structures of **1**−**3** were analyzed by single-crystal X-ray diffraction, and a detailed description of their crystal structures is described.[28] The bulk compositions were confirmed by ^{1}H NMR, elemental analysis, and infrared (IR) spectroscopy. The anticancer activities against lung and oral cancer cell lines and antibacterial activity were also performed to check their therapeutic potential.

RESULTS AND DISCUSSION

Synthesis. Reactions of phen with $\mathbf{dcf}^{-}\mathbf{M}^{+}$ (M = Na, K) in MeOH produced dinuclear complexes of both sodium (**1**) and potassium (**2**). In the presence of LiCl, a mononuclear lithium complex (**3**) was isolated (Figure 1). All three complexes were characterized by single-crystal X-ray diffraction, elemental analysis, UV−vis and IR spectroscopy, and mass spectrometry (MS) (ESI^+). Single crystals were grown directly from the mother liquor.

Analytical Data and Spectral Characterization. Complexes **1**−**3** were obtained in good yield (80−85%) in an analytically pure form. Compounds **1**−**3** melt between 230 and 283 °C. The complexes are soluble in water, methanol, and dimethyl sulfoxide (DMSO). The crystals of complex **1** proved slightly hygroscopic, absorbing small quantities of water upon standing, but otherwise all three complexes appeared to be air stable. In all cases, the empirical formula and composition of the products could be easily established from the analytical data.

Fourier Transform IR. The IR spectra of complexes **1**−**3** are presented in Figure S1 of the Supporting Information, where the broad peaks (2920−3619 cm^{-1}) are due to the O−H stretching frequency, which is broadened because of hydrogen bonding. The carbonyl peaks fall in the range 1590−1650 cm^{-1}, in good agreement with literature examples.[36] The peaks in the range 1512−1515 cm^{-1} reflect the presence of the heterocyclic phen C−N stretching in the complexes.[37]

UV−Vis. Attempts to measure the UV−vis data for complexes **1**−**3** in noncoordinating solvents were hampered by insolubility. As a consequence, the UV−vis data for

DOI: 10.1021/acsomega.9b03314
ACS Omega 2019, 4, 21559−21566

complexes were measured in water. The UV−vis spectra of **1**−**3** are dominated by intense $\pi-\pi^*$ ligand-centered absorption bands at 225 and 265 nm, which are attributed to **phen**-based transitions compared with that of the free ligands (Figure S2). The increase of absorption coefficient (ε) of complexes **1**−**3** (ε = 54 766−112 845 M^{-1} cm^{-1}) compared to that of free ligands (ε_{phen} = 41 850) at 225 nm supports the suggestion that these ligands remain coordinated in solution, with metal coordination enhancing the extinction coefficient.

^{1}H NMR and ^{13}C NMR. NMR spectra of molecules involved in a self-assembly process usually provide useful information about the resulting structure of metal complexes in solution because of upfield/downfield shifts in chemical shifts. In the case of alkali metals, because of weak interaction with the ligand, this shift is usually small compared to transition metal complexes. This could be due to less paramagnetic character associated with alkali metals. Attempts to record NMR data in noncoordinating solvents were again hampered by the insolubility of complexes (vide supra); thus, ^{1}H and ^{13}C NMR spectra of free ligands and complexes **1**−**3** were recorded in DMSO-d_6 (Figures S3−S4). On comparing the peaks of **phen** and Na(**dcf**) with those of complexes **1**−**3**, it was observed that all the signals of the free ligands are present in the ^{1}H NMR spectra of the complexes, that is, four signals for the **phen** and nine more signals for the **dcf**$^-$ protons. Integration assisted in the assignment of the ^{1}H NMR resonances and predicted that the ratio between **dcf**$^-$ and **phen** is 1:1. The signals for the **phen** protons H_a, H_b, and H_d are practically unchanged, while there is a small downfield shift of 0.04−0.05 ppm of the H_c proton (located at para position to the coordinated **phen** N-atom) in all three complexes compared to that of free **phen** (Figure S3, Table S1) and consistent with metal coordination, supported by MS studies (below). The resonance for the N−H proton of **dcf**$^-$ becomes either deshielded (in the case of **1** and **2**) or shielded (in the case of **3**), indicating some binding of the anion to the metal ion in solution.

The ^{13}C NMR of complexes remain unchanged in complexes **1** and **3** compared to that of free ligands; however, there is an upfield shift of δ = 0.9 ppm in the carboxylate carbon of **dcf**$^-$, which indicates that **dcf**$^-$ might be coordinated with K^+ in the solution (Figure S4). Another useful analysis is the 2D NMR experiment where through-space coupling could provide important structural information in solution. However, the 2D spectra did not show any coupling (Figures S5−S7) for complexes **1**−**3**, indicating that either dissociation of the ligands from the alkali metal ions or the coordination environment at the alkali metal precludes the close approach between **phen** and **dfc**$^-$ ligands necessary to observe through-space interactions.

ESI−MS. ESI−MS studies were conducted on all three complexes in MeOH (Figures S8−S10) and all reveal ions corresponding to **phen** H^+, [M(**phen**)]$^+$, and/or [M(**phen**)$_2$]$^+$, clearly indicating that the **phen** remains bound to the alkali metal in solution. While the ^{1}H NMR data clearly point to some ion pairing between the alkali metal and the **dcf**$^-$ anion, there is scant evidence for this in the ESI−MS positive ion spectrum, the exception being a low-intensity peak in the positive ion ESI−MS spectrum of **1** corresponding to [Na(**dcf**) + H]$^+$, suggesting predominant cleavage of the cation−anion bond in the MS studies.

Cumulatively, the UV−vis and MS data reflect coordination of the **phen** ligand to the alkali metal ions in solution, while the ^{1}H NMR data indicate some sensitivity of the N−H proton to the alkali metal reflecting some form of cation−anion pairing in solution.

Crystal Structure Description. *[Na$_2$(phen)$_2$(H$_2$O)$_4$][dcf]$_2$ (1).* The molecular structure of **1** is shown in Figure 2, and

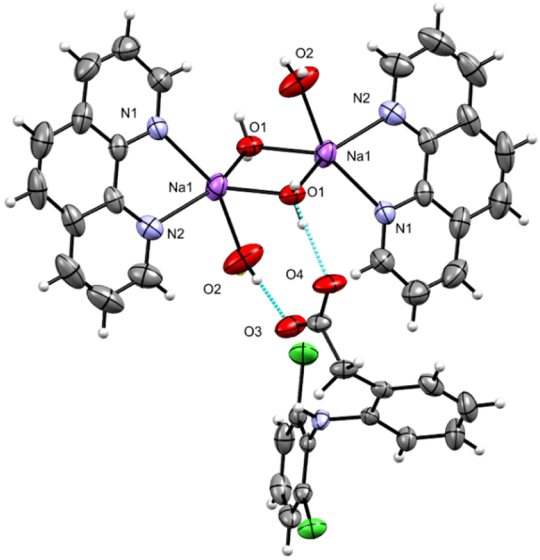

Figure 2. Molecular structure of [Na$_2$(**phen**)$_2$(H$_2$O)$_4$][**dcf**]$_2$ (**1**); thermal ellipsoids are drawn at the 50% probability level.

selected interatomic distances and angles are listed in Table 2. The complex crystallizes in the triclinic space group P-1 with half of the molecule in the asymmetric unit. The Na^+ cations are charge-balanced by two **dcf**$^-$ anions to satisfy the overall charge balance on the complex. Each Na^+ cation is five-coordinated and adopts a distorted spherical square-pyramidal geometry (vide infra), with the O1 water atom occupying the axial position. The equatorial sites comprise two chelating **phen** N (N_{phen}) atoms (N1 and N2) and two water O atoms [(O2 and symmetry-related O1i) symmetry code: $-x+1, -y+1, -z+1$]. The Na−N_{phen} distances [2.491 (2) and 2.433 (2) Å] are consistent with related pentacoordinated Na complexes.[38] **phen** ligand molecules in **1** are planar and have similar bond distances and angles compared to those found in the structure of free **phen**.[39] The two crystallographically identical Na^+ are connected to each other via two bridging water ligands [Na1−O1 = 2.411 (2) Å and Na1−O1−Na1i = 83.50 (7)°], leading to a Na···Na separation of 3.208 (2) Å. The calculation of the degree of distortion of the [NaN_2O_3] coordination polyhedron with respect to an idealized five-coordinate polyhedron by the continuous shape measure (CshM) theory utilizing SHAPE software[28] (vide supra) indicated that the arrangement is closest to the spherical square pyramidal (SPY-5), with a deviation from the ideal C_{4v} symmetry of 2.834 (Figure S11 and Table S2 in the Supporting Information). Sodium complexes containing both **phen** and **dcf** are unknown (CSD 2018). A similar complex with formula [Na$_2$(**2-benzoylbenzoato**)$_4$ (**phen**)$_2$(H$_2$O)$_2$]·H$_2$O is reported,[40] in which the coordination geometry around Na^+ is quite similar to that found in **1**; however, **2-benzoylbenzoate** is coordinated with Na^+, while in **1**, the **dcf**$^-$ remains uncoordinated (vide supra).

[K$_2$(phen)$_2$(dcf)$_2$(H$_2$O)$_4$] (2). The molecular structure of **2** is shown in Figure 3, and selected interatomic distances and

DOI: 10.1021/acsomega.9b03314
ACS Omega 2019, 4, 21559−21566

Table 1. Crystallographic Structural Data for Complexes 1−3

	1	2	3
Crystal Data			
chemical formula	$C_{52}H_{44}Cl_4N_6Na_2O_8$	$C_{52}H_{44}Cl_4K_2N_6O_8$	$C_{26}H_{22}Cl_2LiN_3O_4$
MW	1068.71	1100.93	518.30
crystal system, space group	triclinic, P-1	triclinic, P-1	triclinic, P-1
temperature (K)	296	296	296
a, *b*, *c* (Å)	7.7547 (16), 10.787 (3), 15.807 (4)	7.7271 (15), 11.280 (3), 15.239 (3)	7.8276 (5), 10.9241 (8), 15.0459 (12)
α, *β*, *γ* (deg)	99.936 (10), 100.078 (9), 103.314 (9)	95.707 (11), 100.032 (10), 100.209 (10)	102.434 (4), 95.580 (3), 99.362 (3)
V (Å^3)	1235.1 (5)	1275.6 (5)	1227.92 (16)
Z	1	2	2
μ (mm^{-1})	0.32	0.46	0.30
T_{min}, T_{max}	0.678, 0.745	0.681, 0.745	0.639, 0.745
no. of measured, independent and observed [$I > 2\sigma(I)$] reflections	37 250, 5043, 3922	36 149, 5170, 3786	35 428, 5003, 3631
R_{int}	0.040	0.044	0.056
$(\sin\theta/\lambda)_{max}$ (Å^{-1})	0.625	0.625	0.625
$R[F^2 > 2\sigma(F^2)]$, $wR(F^2)$, S	0.047, 0.121, 1.06	0.051, 0.158, 1.04	0.061, 0.151, 1.06
no. of reflections	5043	5170	5003
no. of parameters	337	341	338
no. of restraints	3	5	4
$\Delta\rho_{max}$, $\Delta\rho_{min}$ (e Å^{-3})	+0.53, −0.55	+0.55, −0.40	+0.37, −0.51
CCDC	1 945 208	1 945 209	1 945 210

Table 2. Selected Geometric Parameters (Å, deg) for 1[a]

Na1−O2	2.334 (2)	Na1−N2	2.433 (2)
Na1−O1i	2.406 (2)	Na1−N1	2.491 (2)
Na1−O1	2.411 (2)	Na1−Na1i	3.208 (2)
O2−Na1−O1i	82.63 (8)	O2−Na1−N1	157.10 (10)
O2−Na1−O1	85.75 (8)	O1i−Na1−N1	115.12 (7)
O1i−Na1−O1	96.51 (7)	O1−Na1−N1	105.32 (7)
O2−Na1−N2	92.98 (10)	N2−Na1−N1	67.55 (7)
O1i−Na1−N2	112.01 (8)	Na1i−O1−Na1	83.49 (7)
O1−Na1−N2	151.08 (8)		

[a]Symmetry code: (i) $-x + 1, -y + 1, -z + 1$.

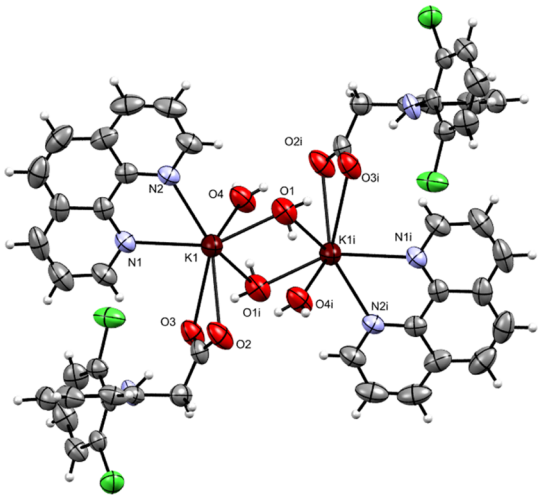

Figure 3. Molecular structure of $[K_2(\mathbf{phen})_2(\mathbf{dcf})_2(H_2O)_4]$ (**2**); thermal ellipsoids are drawn at the 50% probability level.

angles are listed in Table 3. The complex crystallizes in the triclinic space group P-1, with one **phen**, a **dcf**$^-$, a K$^+$ cation, and two coordinated water molecules in the asymmetric unit. The K$^+$ cations are charge-balanced by two **dcf**$^-$ anions, which

Table 3. Selected Geometric Parameters (Å, deg) for 2[a]

K1−O1	2.742 (3)		
K1−N1	2.767 (3)	K1−O1ii	3.100 (3)
K1−N2	2.782 (3)	K1−O3ii	3.187 (3)
K1−O4i	2.873 (3)	K1−O4iii	3.407 (3)
K1−O2ii	2.949 (3)		
O1−K1−N1	147.60 (9)	O2ii−K1−O1ii	72.20 (8)
O1−K1−N2	88.94 (8)	O1−K1−O3ii	131.80 (8)
N1−K1−N2	59.17 (7)	N1−K1−O3ii	80.01 (7)
O1−K1−O4i	77.19 (9)	N2−K1−O3ii	139.15 (7)
N1−K1−O4i	106.36 (8)	O4i−K1−O3ii	100.37 (7)
N2−K1−O4i	90.52 (8)	O2ii−K1−O3ii	41.60 (6)
O1−K1−O2ii	103.78 (8)	O1ii−K1−O3ii	51.33 (7)
N1−K1−O2ii	98.26 (7)	O1−K1−O4iii	54.53 (8)
N2−K1−O2ii	139.51 (8)	N1−K1−O4iii	148.89 (7)
O4i−K1−O2ii	129.57 (9)	N2−K1−O4iii	137.50 (7)
O1−K1−O1ii	92.37 (9)	O4i−K1−O4iii	100.10 (7)
N1−K1−O1ii	117.06 (8)	O2ii−K1−O4iii	51.41 (6)
N2−K1−O1ii	146.60 (8)	O1ii−K1−O4iii	64.97 (8)
O4i−K1−O1ii	57.46 (9)	O3ii−K1−O4iii	79.40 (7)

[a]Symmetry codes: (i) $-x + 2, -y + 1, -z + 1$; (ii) $-x + 1, -y + 1, -z + 1$; (iii) $x - 1, y, z$; (iv) $x + 1, y, z$.

satisfy the overall charge on complex **2**. Each K$^+$ adopts a distorted seven-coordinated geometry comprising a $[N_2O_5]$ donor set. The **phen** ligand adopts *a N,N′*-chelate mode through the N1 and N2 atoms, making a five-membered ring, with K−N distances of 2.767 (2) and 2.782 (2) Å. Like in complex **1**, the K$^+$ lies planar to the **phen** mean planes. The K−N bond lengths lie within the normal observed range of 2.748(4)−2.872 (2) Å for related potassium complexes with **phen** ligands.[41] **dcf**$^-$ coordinates with K$^+$ using both of its carboxylate oxygen atoms (O2 and O3) with K−O bond lengths of 2.949 (3) and 3.187 (2) Å. The K1— O_{water} (O1, O4) distances are 2.742 (3) and 3.100 (4) Å, respectively, while K1−O1/O1i−K1i angles are = 87.63 (9)°, leading to

DOI: 10.1021/acsomega.9b03314
ACS Omega 2019, 4, 21559−21566

K···Ki [symmetry code (i) = $-x + 1, -y + 1, -z + 1$] separation of 4.053 (1) Å. Potassium complexes of **phen** with carboxylate as coligands are not common. A CSD search (2018) resulted in only one hit,[42] in which the K^+ cation appeared to be eight coordinate and $K-O_{carboxylate}$ distances [2.351 (3)−2.488 (2) Å] are quite lower than those observed in **2**. In addition, the K^+ is bridged by carboxylate oxygen compared to complex **2** where K^+ cations are bridged by water molecules (vide infra). The calculation of the degree of distortion of the $[KN_2O_5]$ coordination polyhedron with respect to an idealized five-coordinated polyhedron by the CshM theory (vide supra) indicated that the arrangement appeared to be close to the capped trigonal prism(CTPR-7) with a deviation from the ideal symmetry of 10.00 (Figure S12 and Table S3 in the Supporting Information).

[Li(phen)$(H_2O)_2$][dcf] ***(3)***. The molecular structure of **3** is shown in Figure 4, and selected interatomic distances and angles are listed in Table 4. The complex crystallizes in the triclinic space group P-1, with one **phen** ligand, a Li^+ cation, two coordinated water molecules, and a **dcf**$^-$ anion in the asymmetric unit. The Li^+ cation is charge-balanced by an uncoordinated **dcf**$^-$ anion to satisfy the overall charge balance on the complex. The **phen** ligand molecules are virtually planar, and the values of the bond distances and angles are comparable to those found in the structure of free **phen**.[39] The Li^+ ion adopts a four-coordinated geometry comprising a $[N_2O_2]$ donor set. The bond angles around Li^+ are in the range 81.2 (2)−130.6 (3)°. The **phen** ligand adopts a *N*,*N*′-chelate mode through the N1 and N2 atoms, making a five-membered ring, with Li−N distances of 2.044 (7) and 2.107 (6) Å. The Li−N bond lengths lie within the normal observed range of 2.04−2.29 Å for related lithium complexes with **phen** ligands.[18] The $Li-O_{water}$ distances are 1.921 (5) and 1.936 (7) Å, consistent with hydrated Li^+ complexes reported by others.[18] The degree of distortion of the $[LiN_2O_2]$ coordination polyhedron with respect to an ideal four-coordinated polyhedron was calculated by the CshM theory, which indicated that the arrangement is closest to tetrahedron (T-4), with a deviation from the ideal T_d symmetry of 3.75 (Figure S13 and Table S4 in the Supporting Information). Lithium complexes containing both **phen** and **dcf** are unknown. A CSD search (2018) on lithium complexes with **phen** and carboxylates resulted in two hits;[27,43] in both cases, unlike complex **3**, the carboxylate oxygens are coordinated with Li^+ cations.

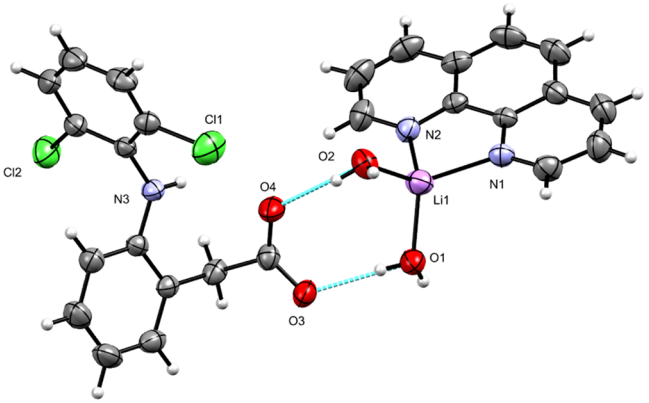

Figure 4. Molecular structure of [Li(**phen**)$(H_2O)_2$][**dcf**] (**3**); thermal ellipsoid are drawn at the 50% probability level.

Table 4. Selected Geometric Parameters (Å, deg) for 3

N1−Li1	2.108 (6)	Li1−O1	1.936 (6)
Li1−O2	1.921 (6)	Li1−N2	2.044 (6)
C12−N1−Li1	110.4 (3)	O2−Li1−N1	130.6 (3)
O2−Li1−O1	103.2 (3)	O1−Li1−N1	112.2 (3)
O2−Li1−N2	107.0 (3)	N2−Li1−N1	81.2 (2)
O1−Li1−N2	123.3 (3)		

Bioactivity of Complexes 1−3. For complexes **1** and **3**, the **dcf**$^-$ anion is hydrogen-bonded to the cation, whereas for complex **2**, the **dcf**$^-$ anion directly bonds to the K^+ cation in the solid state. In polar solvents and those capable of being involved in hydrogen bonding, the species present in solution may well be charge-separated. The solution studies reveal a strong affinity for the **phen** ligand to remain bound to the alkali metal, and ^{1}H NMR shows some sensitivity of the **dcf**$^-$ N−H chemical shift to the metal ion as well. The dominant peaks in the ESI−MS point to the lower molecular weight species present in solution, suggesting that the dimeric motifs evident for both **1** and **2** in the solid state may break down in the presence of donor solvents, with active species being $[M(\textbf{phen})(H_2O)_n]^+$ and/or $[M(\textbf{phen})(\textbf{dcf})(H_2O)_n]$. The complexes' stability was checked in solution periodically by ^{1}H NMR in DMSO-d_6 solvent and always gave the same data.

Anticancer Activity of Metal Complexes. Complexes **1**−**3** were evaluated for anticancer potential against oral (CAL-27) and lung (NCI-H460) cancer cell lines as well as for cytotoxic activities against normal mouse fibroblast (NIH-3T3). As a result, all complexes displayed significant anticancer activities against both cancer cell lines but less cytotoxicity against normal cell lines (Table 5). Complex **1** showed most potent anticancer activity toward lung and oral cancer cells with IC_{50} of 1.69 ± 0.02 and 3.87 ± 0.04, respectively, even better than the standard 5-fluorouracil (Table 5). The other two metal complexes (**2** and **3**) also showed significant anticancer activity against lung and oral cancer cells but less toxicity toward normal cells. Complexes **2** and **3** showed comparable activity with standard 5-fluorouracil (Table 5). The cytotoxic activity of complexes was further confirmed by phase contrast microscopy, which revealed apoptotic cells with a round and irregular morphology after 48 h (Figures S14−S17).

Table 5. Percent Inhibitory Concentration of Compounds on Different Cancer and Normal Cell Lines

compounds	CAL-27 IC50 ± S.D	NCI-H460 IC50 ± S.D	NIH-3T3 IC50 ± S.D
dfc$^-$K$^+$	219.54 ± 0.93	211.02 ± 2.48	>250
1	1.69 ± 0.026	3.87 ± 0.04	54.83 ± 2.36
2	2.95 ± 0.37	4.74 ± 0.86	53.49 ± 2.43
3	3.19 ± 1.54	3.52 ± 0.004	135.21 ± 4.96
5-fluorouracil	2.41 ± 0.89	4.54 ± 1.67	>100 μM

Antimicrobial and Antibiofilm Activity of Metal Compounds. Complexes **1**−**3** showed antivirulence properties against Gram-negative strains (*Klebsiella pneumoniae*, *Escherichia coli*, and *Acinetobacter baumannii*) as compared to Gram-positive strains (*Staphylococcus aureus*). **dcf$^-$K$^+$** showed no activity, while all complexes showed biofilm inhibitory

DOI: 10.1021/acsomega.9b03314
ACS Omega 2019, 4, 21559−21566

Table 6. Percent Biofilm Inhibitory Concentration against Pathogenic Microbes

	microorganisms							
	K. pneumonia		*E. coli*		*A. baumannii*		*S. aureus*	
	MBIC		MBIC		MBIC			
compounds	dose (μM)	% inhibition ± S.D	dose (μM)	% Inhibition ± S.D	dose (μM)	% Inhibition ± S.D	dose (μM)	% Inhibition ± S.D
1	250	78.03 ± 0.062	250	76.83 ± 0.009	250	69.782 ± 0.065	500	0.374 ± 0.304
2	250	77.26 ± 0.063	250	72 ± 0.091	250	86.158 ± 0.068	500	−1.497 ± 0.288
3	250	77.91 ± 0.062	250	76.22 ± 0.026	125	87.924 ± 0.073	500	3.306 ± 0.166
dcf$^-$K$^+$	ND							

activities (Table 6). Furthermore, these complexes have potential to inhibit virulence ability of microorganisms as well as inhibit cancer cells and are likely candidates for the development of new drug formulations but will require more detailed studies to understand their mechanism of action.

CONCLUSIONS

We have successfully prepared three new sodium, potassium, and lithium complexes containing both 1,10-phenanthroline and diclofenac. In all three complexes, **phen** coordinates as a bidentate ligand, while the **dcf**$^-$ ligand either remains uncoordinated (in the case of **1** and **3**) or coordinates in a bidentate fashion (in the case of **2**). All complexes showed significant cytotoxic activity against lung (NCI-H460) and oral cancer cell lines (CAL-27) when compared to the normal mouse fibroblast (NIH-3T3). The cytotoxic activity of the complexes was further confirmed by phase contrast microscopy. The complexes showed significant antibacterial and antibiofilm activity against Gram-negative strains (*K. pneumoniae, E. coli,* and *A. baumannii*).

EXPERIMENTAL SECTION

General Considerations. Solvents, ligands, and metal salts were obtained from commercial suppliers and used without further purification.

Physical Measurements. Melting points were determined using a Stanford Research Systems MPA120 EZ-Melt automated melting point apparatus. Elemental compositions were determined on a PerkinElmer 2400 Series II CHNS/O Analyzer. UV−vis spectra were measured on an Agilent 8453 spectrophotometer using 10^{-5} to 10^{-6} M solutions in water in the range 200−400 nm. IR spectra were recorded using a Bruker Alpha FT-IR spectrometer equipped with a platinum single reflection diamond ATR module. The ^{1}H NMR and ^{13}C NMR spectra were recorded on Bruker 600 MHz in DMSO-d_6. ESI−MS spectra were recorded on Agilent Technologies, 6530 Accurate Mass.

X-ray Crystallography. Crystal data are summarized in Table 1. Single crystals of **1**, **2**, and **3** were mounted on a MiTeGen loop with grease and examined on a Bruker D8 VENTURE APEX diffractometer equipped with a photon 100 CCD area detector at 296 (2) K using graphite-monochromated Mo Kα radiation (λ = 0.71073 Å). Data were collected using the APEX-II software,[29] integrated using SAINT[30] and corrected for absorption using a multiscan approach (SADABS).[31] Final cell constants were determined from full least squares refinement of all observed reflections. The structure was solved using intrinsic phasing (SHELXT).[32] All non-H atoms were located in subsequent difference maps and refined anisotropically with SHELXL-2014/7.[33] H-atoms on carbons were added at calculated positions and refined with a riding model. O−H atoms were located in the difference map and refined isotropically with U(iso) riding on O with DFIX constraints applied. The structures of **1**−**3** have been deposited with the CCDC (CCDC deposition numbers 1945208−1945210).

Cell Culture. Cell lines NCI-H460 (lung cancer), CAL-27 (oral cancer), and NIH-3t3 (mouse normal fibroblast) were purchased from American Type Culture Collection and maintained in our institute biobank facility (PCMD, ICCBS, University of Karachi). The cells were grown and passaged in high-glucose Dulbeccos's modified Eagle's medium (Gibco, USA) supplemented with 3.7 g of sodium bicarbonate, 2 mM L-glutamine, 10% fetal bovine serum, and 1% antibiotic solution. The cells were regularly passaged until reaching 70% confluency.

Cell Cytotoxicity Assay. The cytotoxic capabilities of complexes **1**−**3** were evaluated by the 3-(4′,5′-dimethylthiazol-2-yl)-2,5-diphenyltetrazolium bromide (MTT) assay as described previously.[34] Briefly, cells (10 000/well) were seeded in a 96-well plate and incubated overnight at 37 °C. After 24 h, cells were washed, and monolayer was treated with different concentrations of metallic complexes and incubated further for 48 h. After incubation, 10 μL of MTT dye (0.5 mg/mL) was added in each well and incubated for 4 h. The MTT dye was removed carefully after incubation, and insoluble formazan crystals were dissolved in DMSO. Optical density was read at 570 nm, and percent inhibition of cells was calculated. Ez-Fit Enzyme Kinetics software (Perrella Scientific Inc., Amherst, NH, USA) was used to calculate the IC_{50} value of compounds against cancer and normal cell lines.

Phase Contrast Microscopy. Phase contrast microscopy was performed to observe the morphological changes in cells after treatment with complexes **1**−**3**. Cells (0.2 million/well) were seeded in a six-well plate and incubated for 24 h to form monolayers. Next day, the monolayer was washed and treated with IC_{50} and IC_{70} doses of compounds. The wells were photographed at 0, 24, and 48 h of treatment under a phase contrast microscope (Nikon, Tokyo, Japan) using 10× magnification.

Antimicrobial and Biofilm Inhibitory Concentrations. For antimicrobial and biofilm inhibition assays, *S. aureus* (NCTC 6571), *K. pneumoniae* (ATCC 13882), *A. baumannii* (ATCC 19606), and *E. coli* (ATCC 25922) were used. Microorganisms were grown and maintained by using tryptone soya broth and agar plate (Oxoid, UK). Antimicrobial activity and biofilm inhibition were determined according to CLSI standards and as described before.[35] Briefly, complexes **1**−**3** were twofold serially diluted (500−1 μM) in TSB using a 96-well plate. The above-mentioned bacteria were inoculated at 5 x 10^5 CFU/mL in each well except the negative control. After inoculation, the plate was incubated for 24 h at 37 °C. Next

DOI: 10.1021/acsomega.9b03314
ACS Omega 2019, 4, 21559−21566

day, a clear visible well with the lowest concentration of the compound was considered as minimum inhibitory concentration (MIC).

For the evaluation of biofilm inhibition capability of complexes, a crystal violet biofilm assay was used. Plates were prepared similarly as mentioned in the MIC determination. After overnight incubation, the used media were discarded, and the plate was washed with sterilized distilled water to remove unbound cells. Crystal violet (200 μL; 0.1% w/v) was used to stain biofilms for 15 min after compound treatment. The stain was removed, and the plate was washed to remove excess stain and plates were air-dried. Bound dye was solubilized by using 30% (v/v) glacial acetic acid, and the absorbance was recorded at 590 nm. Biofilm percent inhibition was evaluated by using the formula

$$\text{Percent (\%) biofilm inhibition} = 100 - (\text{abs of treated well/abs of control}) \times 100$$

Synthesis of the Complexes. *$[Na_2(phen)_2(H_2O)_4][dcf]_2$ (1).* **dcf$^-$Na$^+$** (0.319 g, 1 mmol) and **phen** (0.198 g, 0.1 mmol) were refluxed together in MeOH (15 mL) for 2 h. The reaction mixture was cooled to room temperature, filtered, and left undisturbed for crystallization at room temperature. Light pink crystals appeared after 2 weeks (yield: 0.43 g, 83%). mp = 230 °C. UV−vis (5×10^{-6} M, H_2O; λ_{max}, nm; ε, M^{-1} cm^{-1}): 225 (84 232) 266 (57 344). Selected IR data (cm^{-1}): ν_{OH} = 3000−3568, $\nu_{C=O}$ = 1650, $\nu_{C=N}$ = 1508. ^{1}H NMR (600 MHz, DMSO-d_6): δ 10.35 (NH), 9.08 (2H, d), 8.50 (2H, d), 7.99 (2H, s), 7.76−7.78 (2H, q), 7.42 (2H, d), 7.02−7.04 (2H, m), 6.90 (1H, t), 6.71 (1H, t), 6.22 (1H, d), 3.37 (2H, s). ^{13}C NMR (150 MHz, DMSO-d_6): δ 174.9, 150.1, 145.4, 143.4, 138.3, 136.4, 130.0, 129.1, 129.0, 128.6, 128.5, 126.7, 125.6, 123.8, 123.4, 119.7, 115.4, 44.8. Anal. Calcd for $C_{52}H_{44}Cl_4N_6Na_2O_8{\cdot}H_2O$ (%): C, 57.45; H, 4.27; N, 7.74. Found: C, 57.27; H, 4.03; N, 7.61.

$[K_2(phen)_2(dcf)_2(H_2O)_4]$ (2). **dcf$^-$K$^+$** (0.335 g, 1 mmol) and **phen** (0.198 g, 0.1 mmol) were refluxed for 2 h in MeOH (15 mL). The resultant clear solution was cooled to room temperature, filtered, and left undisturbed for crystallization. Colorless crystals suitable for single-crystal X-ray analysis were collected after 2 weeks (yield: 0.453 g, 85%). mp = 283 °C. UV−vis (5.2×10^{-6} M, H_2O; λ_{max}, nm; ε, M^{-1} cm^{-1}): 225 (112 845) 265 (76 151). Selected IR data (cm^{-1}): ν_{OH} = 2900−3610, $\nu_{C=O}$ = 1604, $\nu_{C=N}$ = 1502. ^{1}H NMR (600 MHz, MeOH-d_3): δ 10.65 (NH), 9.09 (2H, d), 8.49 (2H, d), 7.98 (2H, s), 7.75−7.77 (2H, q), 7.42 (2H, d), 7.00−7.03 (2H, m), 6.88 (1H, t), 6.69 (1H, t), 6.20 (1H, d), 3.33 (2H, s). ^{13}C NMR (150 MHz, DMSO-d_6): δ 174.1, 150.0, 145.5, 143.5 138.4, 136.3, 130.0, 129.0, 128.9, 128.8, 128.5, 126.7, 125.4, 123.6, 123.4, 119.6, 115.3, 45.4. Anal. Calcd for $C_{52}H_{44}Cl_4K_2N_6O_8$ (%): C, 56.73; H, 4.03; N, 7.63. Found: C, 56.81; H, 3.94; N, 7.58.

$[Li(phen)(H_2O)_2][dcf]$ (3). **dcf$^-$Na$^+$** (0.0382 g, 1 mmol), **phen** (0.198 g, 0.1 mmol), and LiCl (0.0423 g, 1 mmol) were refluxed for 1 h in MeOH (15 mL). The resultant clear solution was cooled to room temperature, filtered, and left undisturbed for crystallization. Colorless crystal suitable for single-crystal X-ray analysis were collected after 2 weeks (0.415 g, 80%). mp = 250 °C. UV−vis (1.0×10^{-5} M, H_2O; λ_{max}, nm; ε, M^{-1} cm^{-1}): 225 (54 766) 265 (36 884). Selected IR data (cm^{-1}): ν_{OH} = 3090−3568, $\nu_{C=O}$ 1590, $\nu_{C=N}$ = 1515. ^{1}H NMR (600 MHz, DMSO-d_6): δ 10.22 (NH), 9.08 (2H, d), 8.49 (2H, d), 7.98 (2H, s), 7.75−7.77 (2H, q), 7.42 (2H, d), 7.02−7.04 (2H, m), 6.90 (1H, t), 6.71 (1H, t), 6.22 (1H d), 3.38 (s). ^{13}C NMR (150 MHz, DMSO-d_6): δ 174.8, 150.0, 145.5, 143.4, 138.2, 136.3, 136.3, 130.1, 129.0, 128.9, 128.6, 128.5, 126.7, 125.6, 123.8, 123.4, 119.8, 115.5, 44.9. Anal. Calcd for $C_{26}H_{22}C_{l2}LiN_3O_4$ (%): C, 60.25; H, 4.28; N, 8.11. Found: C, 60.25; H, 4.25; N, 8.08.

■ ASSOCIATED CONTENT

Supporting Information

The Supporting Information is available free of charge at https://pubs.acs.org/doi/10.1021/acsomega.9b03314.

Copies of analytical data/spectra, shape analysis, and phase contrast microscopic images for complexes **1**−**3** (PDF)

Crystallographic data of **1**−**3** (CIF)

■ AUTHOR INFORMATION

Corresponding Authors

*E-mail: usman.anwar@unizwa.edu.om (M.U.A.).

*E-mail: aharrasi@unizwa.edu.om (A.A.-H.).

ORCID

Muhammad U. Anwar: 0000-0003-4740-5737

Notes

The authors declare no competing financial interest.

■ ACKNOWLEDGMENTS

The authors would like to thank the University of Nizwa and The Oman Research Council (TRC) for their generous support.

■ DEDICATION

This paper is dedicated to Prof. Annie Powell (KIT, Germany) on the occasion of her 60th birthday.

■ REFERENCES

(1) Elder, D. E.; Massi, D.; Scolyer, R. A.; Willemze, R. *WHO Classification of Skin Tumours*; International Agency for Research on Cancer, 2018.

(2) O'Neill, J. I. M. Antimicrobial Resistance: Tackling a Crisis for the Health and Wealth of Nations. *Rev. Antimicrob. Resist* **2014**, *20*, 1−16.

(3) Li, B.; Webster, T. J. Bacteria Antibiotic Resistance: New Challenges and Opportunities for Implant-associated Orthopedic Infections. *J. Orthop. Res.* **2018**, *36*, 22−32.

(4) Bowler, P. G. Antibiotic Resistance and Biofilm Tolerance: A Combined Threat in the Treatment of Chronic Infections. *J. Wound Care* **2018**, *27*, 273−277.

(5) Ventola, C. L. The Antibiotic Resistance Crisis: Part 1: Causes and Threats. *Pharm. Therapeut.* **2015**, *40*, 277.

(6) Turel, I.; Kljun, J. Interactions of Metal Ions with DNA, Its Constituents and Derivatives, Which May Be Relevant for Anticancer Research. *Curr. Top. Med. Chem.* **2011**, *11*, 2661−2687.

(7) Arunadevi, A.; Porkodi, J.; Ramgeetha, L.; Raman, N. Biological Evaluation, Molecular Docking and DNA Interaction Studies of Coordination Compounds Gleaned from a Pyrazolone Incorporated Ligand. *Nucleosides, Nucleotides Nucleic Acids* **2019**, *38*, 656−679.

(8) Bharti, S. K.; Singh, S. K. Metal Based Drugs: Current Use and Future Potential. *Der Pharm. Lett.* **2009**, *1*, 39−51.

(9) Zamble, D. B.; Lippard, S. J. Cisplatin and DNA Repair in Cancer Chemotherapy. *Trends Biochem. Sci.* **1995**, *20*, 435−439.

(10) Cao, Q.; Yang, J.; Zhang, H.; Hao, L.; Yang, G. G.; Ji, L. N.; Mao, Z. W. Traceable In-Cell Synthesis and Cytoplasm-to-Nucleus

DOI: 10.1021/acsomega.9b03314
ACS Omega 2019, 4, 21559−21566

Translocation of a Zinc Schiff Base Complex as a Simple and Economical Anticancer Strategy. *Chem. Commun.* **2019**, *55*, 7852.
(11) Awwad, N. S.; Saleh, K. A.; Abbas, H.-A. S.; Alhanash, A. M.; Alqadi, F. S.; Hamdy, M. S. Induction Apoptosis in Liver Cancer Cells by Altering Natural Hydroxyapatite to Scavenge Excess Sodium without Deactivate Sodium-Potassium Pump. *Mater. Res. Express* **2019**, *6*, 055403.
(12) Jansson, B. Potassium, Sodium, and Cancer: A Review. *J Environ Pathol Toxicol Oncol.* **1996**, *15*, 65−73.
(13) Baixauli, F.; Villa, M.; Pearce, E. L. Potassium Shapes Antitumor Immunity. *Science* **2019**, *363*, 1395−1396.
(14) Barrett, T.; Riemer, F.; McLean, M. A.; Kaggie, J.; Robb, F.; Tropp, J. S.; Warren, A.; Bratt, O.; Shah, N.; Gnanapragasam, V. J. Quantification of Total and Intracellular Sodium Concentration in Primary Prostate Cancer and Adjacent Normal Prostate Tissue with Magnetic Resonance Imaging. *Invest. Radiol.* **2018**, *53*, 450−456.
(15) Kovacsics, C. E.; Gottesman, I. I.; Gould, T. D. Lithium's Antisuicidal Efficacy: Elucidation of Neurobiological Targets Using Endophenotype Strategies. *Annu. Rev. Pharmacol. Toxicol.* **2009**, *49*, 175−198.
(16) Li, H.; Huang, K.; Liu, X.; Liu, J.; Lu, X.; Tao, K.; Wang, G.; Wang, J. Lithium Chloride Suppresses Colorectal Cancer Cell Survival and Proliferation through ROS/GSK-3β/NF-KB Signaling Pathway. *Oxid. Med. Cell. Longevity* **2014**, *2014*, 1.
(17) Yang, L.-Q.; Fang, D.-C.; Wang, R.-Q.; Yang, S.-M. Effect of NF-KB, Survivin, Bcl-2 and Caspase3 on Apoptosis of Gastric Cancer Cells Induced by Tumor Necrosis Factor Related Apoptosis Inducing Ligand. *World J. Gastroenterol.* **2004**, *10*, 22.
(18) Buttery, J. H. N.; Effendy, G. A.; Koutsantonis, G. A.; Mutrofin, S.; Plackett, N. C.; Skelton, B. W.; Whitaker, A. H. Complexes of Group 1 Salts with N, N′-Aromatic Bidentate Ligands, of Mononuclear ("Molecular") 1: 2 Salt: Base Ratio. *Z. Anorg. Allg. Chem.* **2006**, *632*, 1829−1838.
(19) Ma, C.; Wang, W.; Zhang, X.; Chen, C.; Liu, Q.; Zhu, H.; Liao, D.; Li, L. Molecular, One-and Two-Dimensional Systems Built from Manganese (II) and Phthalate/Diimine Ligands: Syntheses, Crystal Structures and Magnetic Properties. *Eur. J. Inorg. Chem.* **2004**, *2004*, 3522−3532.
(20) Platero-Prats, A. E.; de la Peña-O'Shea, V. A.; Proserpio, D. M.; Snejko, N.; Gutiérrez-Puebla, E.; Monge, Á. Insight into the SBU Condensation in Mg Coordination and Supramolecular Frameworks: A Combined Experimental and Theoretical Study. *J. Am. Chem. Soc.* **2012**, *134*, 4762−4771.
(21) McCann, M.; Santos, A. L. S.; Da Silva, B. A.; Romanos, M. T. V.; Pyrrho, A. S.; Devereux, M.; Kavanagh, K.; Fichtner, I.; Kellett, A. Vitro and in Vivo Studies into the Biological Activities of 1, 10-Phenanthroline, 1, 10-Phenanthroline-5, 6-Dione and Its Copper (II) and Silver (I) Complexes. *Toxicol. Res.* **2012**, *1*, 47−54.
(22) Boumans, H.; van Gaalen, M. C. M.; Grivell, L. A.; Berden, J. A. Differential Inhibition of the Yeast Bc 1Complex by Phenanthrolines and Ferroin Implications For Structure And Catalytic Mechanism. *J. Biol. Chem.* **1997**, *272*, 16753−16760.
(23) Sartorius, C.; Dunn, M. F.; Zeppezauer, M. The Binding of 1, 10-phenanthroline to Specifically Active-site Cobalt (II)-substituted Horse-liver Alcohol Dehydrogenase: A Probe for the Open-enzyme Conformation. *Eur. J. Biochem.* **1988**, *177*, 493−499.
(24) Llinàs, A.; Burley, J. C.; Box, K. J.; Glen, R. C.; Goodman, J. M. Diclofenac Solubility: Independent Determination of the Intrinsic Solubility of Three Crystal Forms. *J. Med. Chem.* **2007**, *50*, 979−983.
(25) Lakshman, T. R.; Deb, J.; Ghosh, I.; Sarkar, S.; Paine, T. K. Combining Anti-Inflammatory and Anti-Proliferative Activities in Ternary Metal-NSAID Complexes of a Polypyridylamine Ligand. *Inorg. Chim. Acta* **2019**, *486*, 663−668.
(26) Echenique-Errandonea, E.; Oyarzabal, I.; Cepeda, J.; San Sebastian, E.; Rodríguez-Diéguez, A.; Seco, J. M. Photoluminescence and Magnetic Analysis of a Family of Lanthanide (III) Complexes Based on Diclofenac. *New J. Chem.* **2017**, *41*, 5467−5475.
(27) Shah, S. R.; Shah, Z.; Ullah, N.; Hussain, J.; Al-Harrasi, R.; Khan, A.; Rawson, J. M.; Al-Harrasi, A.; Anwar, M. U. Crystal Structure, Shape Analysis and Bioactivity of New LiI, NaI and MgII Complexes with 1, 10-Phenanthroline and 2-(3, 4-Dichlorophenyl) Acetic Acid. *Acta Crystallogr., Sect. C: Struct. Chem.* **2019**, *75*, 294.
(28) Llunell, M.; Casanova, D.; Cirera, J.; Alemany, P.; Alvarez, S. *SHAPE*, Version 2.1.; Univ. Barcelona: Barcelona, Spain, 2013; p 2103.
(29) *APEX-II*; Bruker AXS: Madison, WI, USA.
(30) *SAINT*; Bruker AXS: Madison, WI, USA.
(31) *SADABS*; Bruker AXS: Madison, WI, USA.
(32) Sheldrick, G. M. SHELXT- Integrated space-group and crystal-structure determination. *Acta Crystallogr., Sect. A: Found. Adv2E* **2015**, *71*, 3.
(33) *SHELXTL*; Bruker AXS: Madison, Wisconsin, USA, 2015.
(34) Zehra, B.; Ahmed, A.; Sarwar, R.; Khan, A.; Farooq, U.; Abid Ali, S.; Al-Harrasi, A. Apoptotic and Antimetastatic Activities of Betulin Isolated from Quercus Incana against Non-Small Cell Lung Cancer Cells. *Cancer Manage. Res.* **2019**, *11*, 1667.
(35) Ahmed, A.; Khan, A. K.; Anwar, A.; Ali, S. A.; Shah, M. R. Biofilm Inhibitory Effect of Chlorhexidine Conjugated Gold Nanoparticles against Klebsiella Pneumoniae. *Microb. Pathog.* **2016**, *98*, 50−56.
(36) Deacon, G. B.; Phillips, R. J. Relationships between the Carbon-Oxygen Stretching Frequencies of Carboxylato Complexes and the Type of Carboxylate Coordination. *Coord. Chem. Rev.* **1980**, *33*, 227−250.
(37) Neykov, M.; van Almsick, T.; Dimitrov, G. Synthesis, Spectral Properties and Crystal Structure of Calcium and Strontium Complexes of 1, 10-Phenanthroline. *Z. Anorg. Allg. Chem.* **2006**, *632*, 1554−1559.
(38) Zhang, B.; Xie, C.-Z.; Wang, X.-Q.; Shen, G.-Q.; Shen, D.-Z. A Novel Heterometallic FeII−Na+ Phase: 1, 10-Phenanthrolinium Aquabis (1, 10-Phenanthroline) Sodium (I) Pentacyanonitrosoiron (II) Monohydrate. *Acta Crystallogr., Sect. E: Struct. Rep. Online* **2004**, *60*, m1293−m1295.
(39) Tian, Y. P.; Duan, C.-Y.; Xu, X.-X.; You, X.-Z. Screw-Chain Structure of 1, 10-Phenanthroline Hydrate, C12H8N2. H2O. *Acta Crystallogr. Sect. C Cryst. Struct. Commun.* **1995**, *51*, 2309−2312.
(40) Ying-Qun, Y.; Shao-Hua, Z.; Si-Ping, T.; Li-Xia, F. Synthesis, Crystal Structure and Fluorescent Property of One New Complex [Na-2 (2-Benzoylbenzoato)(4)(Phen)(2)(H2O)(2)] Center Dot H2O. *Chin. J. Struct. Chem.* **2013**, *32*, 63−66.
(41) Buttery, J. H. N.; Mutrofin, S.; Plackett, N. C.; Skelton, B. W.; Whitaker, C. R.; White, A. H. Complexes of Group 1 Salts with N, N′-Aromatic Bidentate Ligands, of 1: 1 Salt: Base Ratio. *Z. Anorg. Allg. Chem.* **2006**, *632*, 1809−1828.
(42) Gao, E.; Huang, Y.; Zhu, M.; Wang, L.; Liu, F.; Liu, H.; Ma, S.; Shi, Q.; Wang, N.; Shi, C. A New Binuclear Potassium (I) Complex with a Novel 1D Infinite Water Chain Containing (H2O) 12 Clusters. *Inorg. Chem. Commun.* **2009**, *12*, 872−874.
(43) Hundal, M. S.; Sood, G.; Kapoor, P.; Poonia, N. S. Structure of Lithium (3, 5-Dinitrobenzoate)(1, 10-Phenanthroline) Monohydrate. *J. Chem. Crystallogr.* **1991**, *21*, 395−398.

DOI: 10.1021/acsomega.9b03314
ACS Omega 2019, 4, 21559−21566